

Supplementary material for: Gene regulation inference from single-cell RNA-seq data with linear differential equations and velocity inference

Pierre-Cyril Aubin-Frankowski¹ and Jean-Philippe Vert^{2,1}

¹ MINES ParisTech, PSL Research University,
CBIO - Centre for Computational Biology, F-75006 Paris, France

² Google Brain, F-75009 Paris, France.

1 Assessing the linear ODE model

As recalled in Figure S1, GRISLI combines two successive steps. It first infers a velocity vector \hat{v}_i for each cell i , and then models the expression-velocity relationship with a linear ODE model of the form $\tilde{v}_i \approx \mathbf{A}x_i$, where x_i is the gene expression vector of the i -th cell and \mathbf{A} is the square matrix of regulation. In order to assess how good a linear model fits the expression-velocity relationship, we compare the matrix of velocities $\hat{\mathbf{V}}$ to the best linear approximation $\mathbf{A}\mathbf{X}$, both quantitatively and qualitatively, on both datasets of the Matsumoto benchmark.

Figure S2 (a) and (b) shows, respectively for the murine and human datasets, the estimated velocities $\hat{\mathbf{V}}$ (in red) and the velocities predicted by the linear model $\mathbf{A}\mathbf{X}$ (in blue), mapped in two dimensions by projection onto the first two principal components of the cell expressions. In both cases we note that the velocities $\hat{\mathbf{V}}$ inferred by GRISLI correctly indicate an evolution from the earlier cells to the later cells, and tend to be well correlated with the reconstructed velocities $\mathbf{A}\mathbf{X}$, particularly for the human dataset. This can be ascertained numerically through the coefficient of determination (R^2) statistics, either computed for the whole regression R_{tot}^2 , or TF-wise $(R_j^2)_{j \leq G}$ as follows:

$$R_{\text{tot}}^2 = 1 - \frac{\sum_{i=1}^C \sum_{j=1}^G |\hat{v}_{i,j} - (\mathbf{A}\mathbf{X})_{i,j}|^2}{\sum_{i=1}^C \sum_{j=1}^G |\hat{v}_{i,j} - \bar{v}_j|^2} \quad R_j^2 = 1 - \frac{\sum_{i=1}^C |\hat{v}_{i,j} - (\mathbf{A}\mathbf{X})_{i,j}|^2}{\sum_{i=1}^C |\hat{v}_{i,j} - \bar{v}_j|^2} \quad \text{with } \bar{v}_j = \sum_{i=1}^C \hat{v}_{i,j}.$$

The distribution of R^2 values per TF is presented on Figure S3, for both datasets. We see that for the murine data, the R_j^2 are significantly positive but modest in absolute value (0.25 on average), and while for the human data the R^2 values are much higher (0.75 on average). This is further illustrated on Figure S2(c)-(d) through scatter plots of $((\mathbf{A}\mathbf{X})_j, \hat{\mathbf{V}}_j)$ for the TF j in each dataset with R_j^2 closest to R_{tot}^2 . Overall, these results suggest that, in spite of its simplicity, the linear ODE model captures a significant amount of information in the data.

2 Detailed results on the Matsumoto benchmark

In addition to the AUC values provided in Table 1, Figure S4 shows the ROC and precision-recall curves of SCODE, GRISLI and TIGRESS on both datasets of the Matsumoto benchmark. Tables S1 and S2 show the top 20 regulations predicted by GRISLI trained on the Matsumoto datasets.

While no discernible pattern emerges among the targets, we see that GRISLI predicts as top regulators, Stat1 for the murine data and NANOG and GATA6 for the human data¹. Interestingly the inferred regulator

¹The importance of NANOG and GATA6 in differentiation of human ES cells to fibroblast has been reported in <http://genesdev.cshlp.org/content/29/12/1239.full> <https://www.ncbi.nlm.nih.gov/pubmed/25209243> <https://www.ncbi.nlm.nih.gov/pmc/articles/PMC5550920/> [https://www.cell.com/stem-cell-reports/pdf/S2213-6711\(16\)30316-2.pdf](https://www.cell.com/stem-cell-reports/pdf/S2213-6711(16)30316-2.pdf)

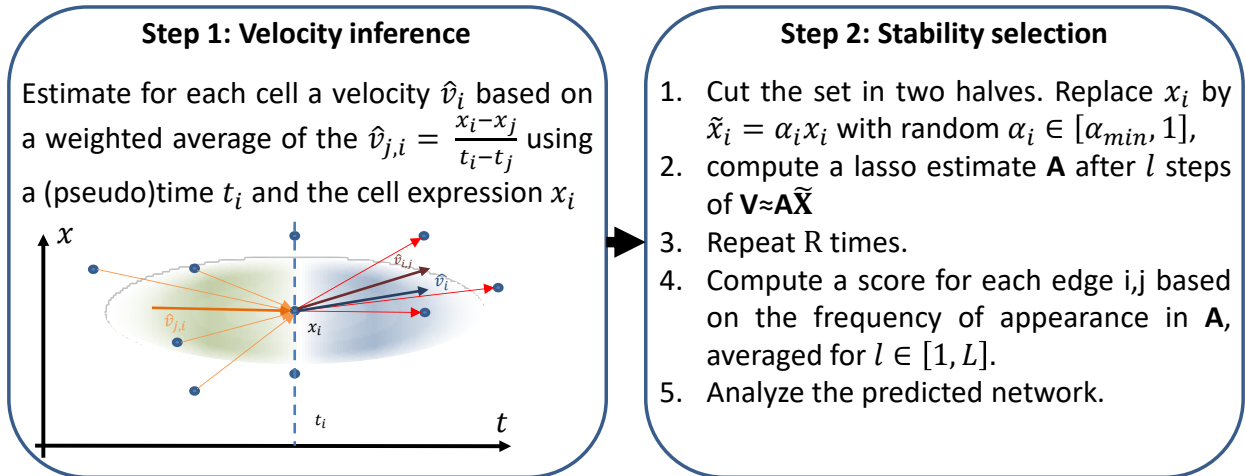


Figure S1: Summary of the two steps of GRISLI

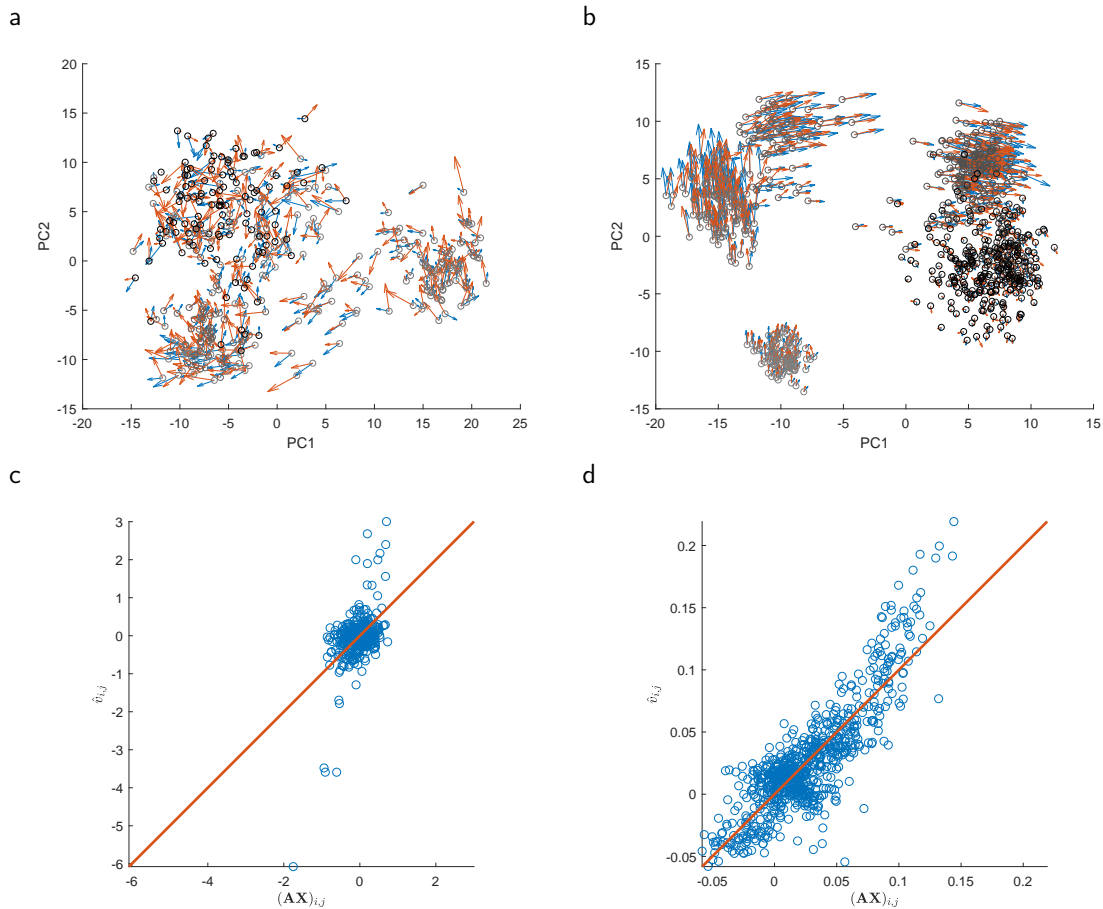


Figure S2: (a) and (b): PCA of scRNA-Seq data for the murine (left) and human (right) benchmarks. Each circle represents a cell, its color representing its experimental time (from light gray to black). The projections of the inferred velocities $\hat{\mathbf{V}}$, and of the reconstructed velocities $\mathbf{A}\mathbf{X}$ are represented by blue and red arrows respectively. (c) and (d): Scatter plots of $((\mathbf{A}\mathbf{X})_j, \hat{\mathbf{V}}_j)$ for one TF j in each dataset with R_j^2 closest to R_{tot}^2 .

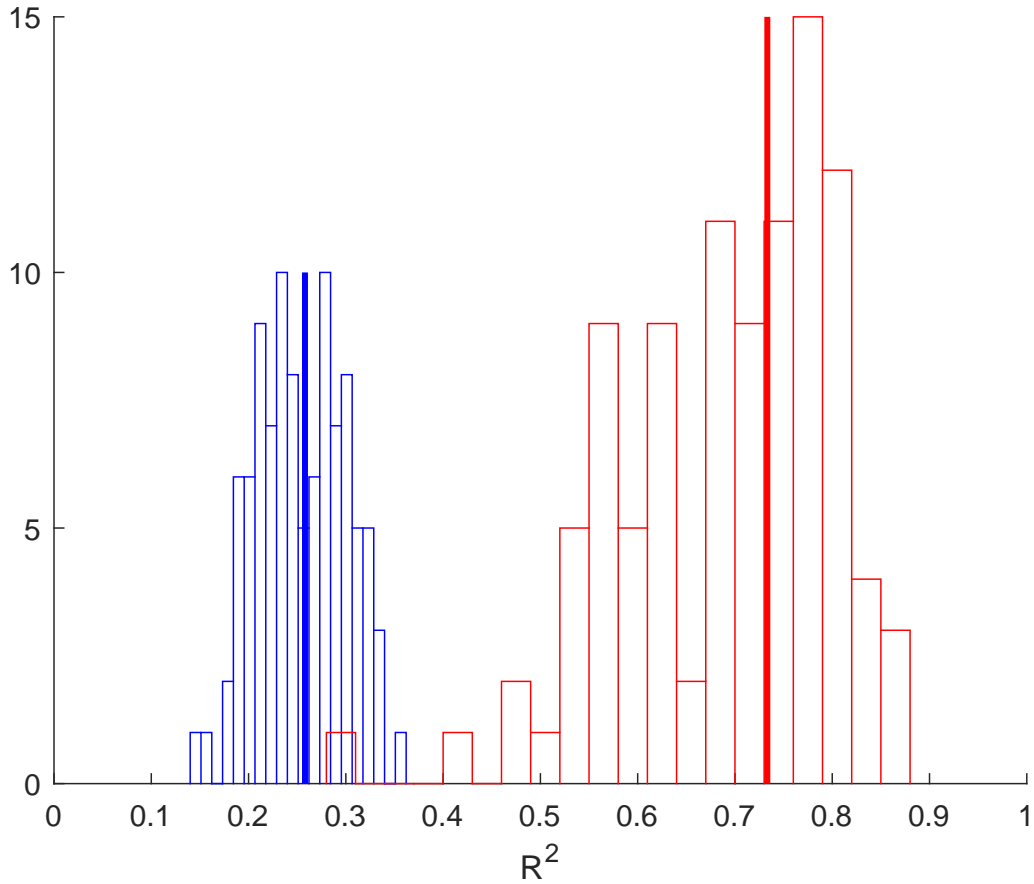


Figure S3: Histogram of the $(R_j^2)_{j \leq G}$ for the murine (blue) and human (red) data. The height of each box represents the number of TF with an R^2 in a given range. The vertical lines correspond to R_{tot}^2 .

TFs with highest score are very different between GRISLI (NANOG, GATA6), GRISLI with ZINB-WaVE imputation (ZEB1, MAF) and SCODE with or without imputation (EOMES).

3 Results on the pancreatic dataset

Similarly, Figure S5 shows the ROC and precision-recall curves of SCODE, TIGRESS and GRISLI with two ways to infer velocities (using the default GRISLI method, or scvelo) on the pancreatic dataset.

Tables S3 and S4 show the top 20 regulations predicted by GRISLI trained on the pancreatic datasets using, respectively, velocities inferred by GRISLI or scvelo.

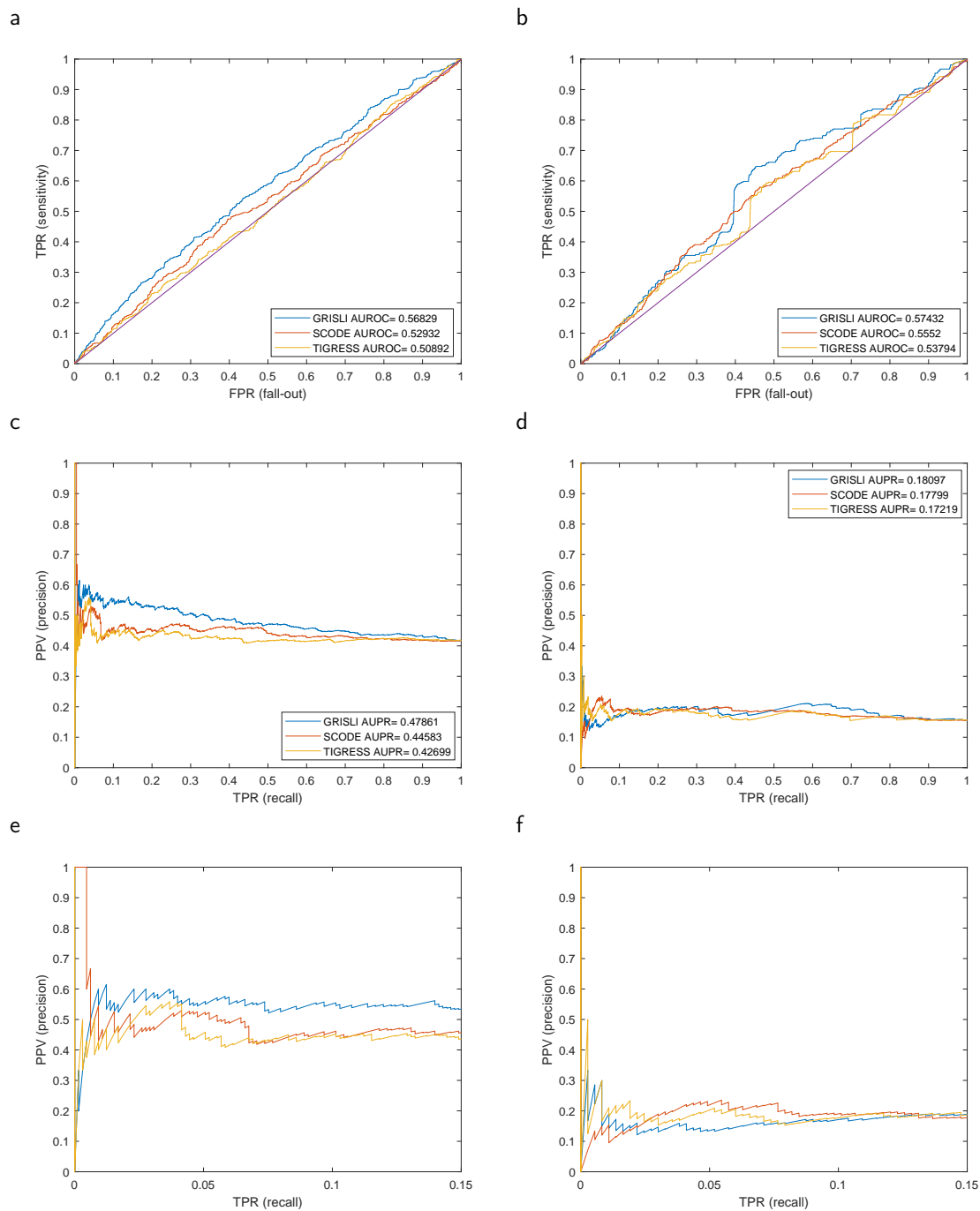


Figure S4: Using the same parameters as in Figure 1: (a): ROC curves for the murine dataset. (b): ROC curves for the human dataset. (c): Precision-recall curves for the murine dataset. (d): Precision-recall curves for the human dataset. (e): Precision-recall curves for the murine dataset at low recall. (f): Precision-recall curves for the human dataset at low recall.

Target	Regulator
Kdm5b	Stat1
Zfhx4	Tet2
Kdm5b	Zfp317
Scx	Stat1
Zfp57	Jun
Hmga1	Trp53
Sox11	Foxs1
Atf3	Mef2c
Klf10	Stat1
Dnajc2	Lyar
Zeb2	Dnajc2
<i>Irf9</i>	<i>Trp53</i>
Fos	Dnajc2
Ncoa1	Dnajc2
Id2	Stat1
Nfe2l1	Dnajc2
<i>Klf4</i>	<i>Nfic</i>
Ezh2	Sp1
Hmga2	Tet2
Noc4l	Nfe2l1

Table S1: The 20 highest-scoring regulations predicted for the murine data by a single run of GRISLI. The regulations present in the gold standard network are in bold, those present in the gold standard but in a reversed order in italics.

Target	Regulator
TCF7L2	NANOG
TFAP2A	GATA6
ZNF587	TBX3
SMAD7	NANOG
ID4	GATA6
TCF7	NANOG
ID2	GATA6
TULP4	NANOG
ETV5	NANOG
SP5	GATA6
FOXF1	ID2
ID3	GATA6
MIER1	NANOG
HAND1	ID2
SMAD2	GATA6
SNAI2	ID2
HOXB6	ID2
ZNF652	NANOG
ZNF516	GATA6
MSX2	NANOG

Table S2: The 20 highest-scoring regulations predicted for the human data by a single-run of GRISLI. The regulations present in the gold standard network are in bold, those present in the gold standard but in a reversed order in italics.

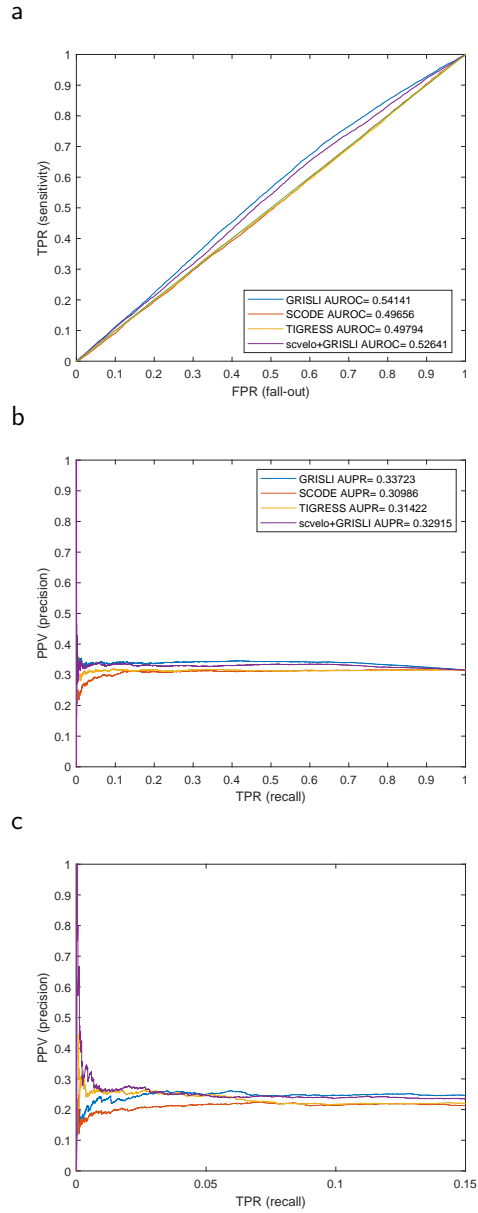


Figure S5: Using the same parameters as in Figure 3: (a): ROC curve for the pancreatic dataset. (b): Precision-recall curve for the pancreatic dataset.(c): Precision-recall curve for the pancreatic dataset at low recall.

Target	Regulator
MTF1	CREB1
<i>PLAG1</i>	<i>RFX3</i>
NR1H4	CREB1
<i>FOXJ3</i>	<i>MEF2D</i>
MEF2D	ATF2
MECP2	TCF12
MECOM	ETV6
PBX1	NEUROD1
GABPB2	GLIS3
PLAG1	HSF1
MECP2	ZFX
LMX1B	SP1
ATF2	MEF2D
MEF2D	RFX3
<i>PAX4</i>	<i>OVOL2</i>
STAT3	PBX2
NFIA	SOX5
<i>CREB1</i>	<i>MEF2D</i>
NR3C1	NR5A2
PLAG1	ELF1

Table S3: The 20 highest-scoring interactions predicted for the pancreatic data by a single-run of GRISLI. The regulations present in the gold standard network are in bold, those present in the gold standard but in a reversed order in italics.

Target	Regulator
<i>NR6A1</i>	<i>E2F1</i>
<i>EGR1</i>	<i>NFATC3</i>
ATF4	NKX2-2
RFX3	HNF4A
ATF4	TGIF2
NR6A1	NR3C1
ATF4	RELA
<i>FOXP1</i>	<i>NR3C1</i>
ATF4	HNF1B
ATF4	ZFP410
PBX3	SP3
<i>NR6A1</i>	<i>THRA</i>
TCF12	SP1
NR6A1	MNX1
FOXP1	HSF1
<i>NKX6-1</i>	<i>MEF2D</i>
PBX3	RORA
FOXP1	CLOCK
<i>ELK3</i>	<i>PBX2</i>
NR6A1	RXRβ

Table S4: The 20 highest-scoring interactions predicted for the pancreatic data by a single-run of GRISLI with scvelo. The regulations present in the gold standard network are in bold, those present in the gold standard but in a reversed order in italics.